AD-A031 232 WASHINGTON UNIV SEATTLE DEPT OF ELECTRICAL ENGINEERING F/G 17/2
THEORETICAL STUDY OF MICROWAVE COUPLING IN AN ELECTROOPTIC DIFF--ETC(U)
MAR 73 R B SMITH, J H HARRIS, W D SCOTT N00953-73-M-0250

UNCLASSIFIED NL

1 OF 1
ADA031232

END

DATE
FILMED
11 -76

UNIVERSITY OF WASHINGTON
COLLEGE OF ENGINEERING
DEPARTMENT OF ELECTRICAL ENGINEERING
SEATTLE, WASHINGTON 98195

Principal Investigators

JAY. H. HARRIS

and

WILLIAM D. SCOTT

Prepared for
Naval Electronic Laboratory Center (Code 2500)
San Diego, California 92152

UNIVERSITY OF WASHINGTON
COLLEGE OF ENGINEERING
DEPARTMENT OF ELECTRICAL ENGINEERING
SEATTLE, WASHINGTON 98195

73
Contract N00953-M-0250

Final Report

THEORETICAL STUDY OF MICROWAVE COUPLING IN AN ELECTROOPTIC DIFFRACTION MODULATOR

R. B. Smith, J. H. Harris

30 March 1973

Principal Investigator

Jay H. Harris

Prepared for

Naval Electronics Laboratory Center
San Diego, California 92152

UNCLASSIFIED

SECURITY CLASSIFICATION OF THIS PAGE (When Data Entered)

REPORT DOCUMENTATION PAGE

READ INSTRUCTIONS BEFORE COMPLETING FORM

1. REPORT NUMBER

2. GOVT ACCESSION NO.

3. RECIPIENT'S CATALOG NUMBER

4. TITLE (and Subtitle)

Theoretical Study of Microwave Coupling in an Electrooptic Diffraction Modulator

5. TYPE OF REPORT & PERIOD COVERED

Final report

6. PERFORMING ORG. REPORT NUMBER

7. AUTHOR(s)

R. B. Smith, J. H. Harris

8. CONTRACT OR GRANT NUMBER(s)

N00953-73-M-0250 NEW

9. PERFORMING ORGANIZATION NAME AND ADDRESS

University of Washington
Department of Electrical Engineering
Seattle, WA 98195

10. PROGRAM ELEMENT, PROJECT, TASK AREA & WORK UNIT NUMBERS

11. CONTROLLING OFFICE NAME AND ADDRESS

Naval Electronics Laboratory Center
Code 2500
San Diego, CA 92452

12. REPORT DATE

30 March 1973

13. NUMBER OF PAGES

40

14. MONITORING AGENCY NAME & ADDRESS (if different from Controlling Office)

15. SECURITY CLASS. (of this report)

UNCLASSIFIED

15a. DECLASSIFICATION/DOWNGRADING SCHEDULE

16. DISTRIBUTION STATEMENT (of this Report)

Approved for public release, distribution unlimited

17. DISTRIBUTION STATEMENT (of the abstract entered in Block 20, if different from Report)

18. SUPPLEMENTARY NOTES

19. KEY WORDS (Continue on reverse side if necessary and identify by block number)

Integrated optics
Microwave
Optical communications
Waveguide

20. ABSTRACT (Continue on reverse side if necessary and identify by block number)

The electrical properties of diffraction modulators are reviewed. Estimates for capacitance and figure of merit (watts per Hz bandwidth) are derived. Emphasis is on geometries with electrode width and spacing approximately equal to isolation layer thickness.

DD FORM 1 JAN 73 1473 EDITION OF 1 NOV 65 IS OBSOLETE
S/N 0102-014-6601

UNCLASSIFIED

SECURITY CLASSIFICATION OF THIS PAGE (When Data Ent...

Introduction

Integrated optical techniques hold promise for providing modulators with bandwidths in excess of those available with conventional bulk devices. In this report we review aspects of the electrical properties of diffraction modulators. Estimates are obtained for the capacitance and figure of merit with particular emphasis on the range of geometric characteristics in which the modulator electrode width and spacing is of comparable dimension with the thickness of isolation layers used to reduce optical absorption by the electrodes.

Realization of wide bandwidth operation is dependent on material properties in both the optical and microwave modulation frequency range. In that regard we also discuss in brief aspects of the absorption properties of polar liquids and methods for the introduction of microwave signals into modulator configurations.

I. Electrical Properties of Diffraction Modulators

The development of wide bandwidth electro-optic modulators is dependent on achieving device designs that result in low voltage, low capacitance structures. In general, the smaller the device the greater is its potential bandwidth. In this section we outline properties of thin film diffraction modulators that are fabricated with interdigital fingers and that employ low index isolation layers to separate metal fingers from the waveguides. Principal interest lies in the capacitance of the device and in the electric field in the active medium. A range of geometric parameters is treated that is consistent with the idea that a practical modulator should have dimensions as small as possible.

The mechanism of modulation in the diffraction modulator is conversion of guided wave energy from one spatial harmonic to one or more others. The width of the device must be sufficient to accommodate the incident beam with some appropriate safety factor. Although the first thin film diffraction modulators[2,3] have contained many finger electrodes, the same concepts of interdigitation and spatial conversion of guided wave energy apply down to linear waveguide structures that are a wavelength in width and contain only two or three fingers. Thus with generally small corrections due to end effects the results that are presented in this section apply to a wide class of thin film electro-optic modulators.

a. Approximate Solution for the Electrode Field

Our interest lies in obtaining approximate solutions for the electric field generated by an interdigital structure immersed in a multilayer dielectric medium (Fig. 1). The problem is treated as a two-dimensional one through neglect of the fringing fields at the end of the fingers. Knowledge of the potential distribution $\Phi(o,y)$ between the fingers is tantamount to a full solution of the problem. Our approach to the determination of capacitance and field parameters is to start with an approximate expression for $\Phi(o,y)$ obtained on the basis of physical arguments. Aspects of the error in the approximation will be discussed in a later report under this contract.

The equipotential surfaces about the fingers of the interdigital structure have an expected appearance resembling that shown in Fig. 2. The fingers themselves may be modeled as elliptic surfaces with major axis approximately equal to the finger width 2b. Near the fingers the equipotential surfaces will also have an elliptic appearance. Our approximate solution for $\Phi(o,y)$ is obtained using the concentric elliptic configuration illustrated in Fig. 2(b) in which the outer ellipse has a major axis of length 2a equal to the distance between finger centers.

The solution for the potential distribution within confocal ellipses is well known[4] and may be deduced from the conformal mapping

$$Z = (y + iz)/b = \cos W = \cos(u + iv) = \cos u \cosh v - i \sin u \sinh v \qquad (1)$$

In (1) v = constant defines the equipotential surfaces. The solution for

the potential distribution is

$$\Phi = (V_o/2)v/\cosh^{-1} a/b \tag{2}$$

with

$$v = \sinh^{-1} [(y'^2 + z'^2 - 1)/2 \pm \{(y'^2 + z'^2 - 1)^2/4 + z'^2\}^{\frac{1}{2}}]^{\frac{1}{2}} \tag{3}$$

and $y' = y/b$, $z' = z/b$. The plus sign in (3) yields zero potential over the inner ellipse ($z=0$, $|y|<b$) and is the desired solution.

The electric field between the electrodes at the interface $z=0$ is of primary concern and is found by differentiation of (3) with the plus sign to be

$$\underline{E} = -(V_o/2 \cosh^{-1} a/b)(y^2 - b^2)^{-\frac{1}{2}} \hat{y}(y/|y|) \tag{4}$$

Note that the dimension b in (4) is properly half the distance between foci of the inner ellipse rather than the semi major axis and that the singularity in (4) is removed for electrodes of finite thickness.

The charge per unit length on the inner conductor may be found from the capacitance of confocal ellipses[4] to be

$$Q = -(V_o/2)\ 2\pi\varepsilon/\cosh^{-1} a/b \tag{5}$$

This expression may be verified by integration over the charge density on the inner conductor. The charge density is found to be

$$\begin{aligned} P_s &= -\varepsilon(\partial\Phi/\partial z)_{z=0} \\ &= -(V_o\varepsilon/2b \cosh^{-1} a/b)(1 - y^2/b^2)^{-\frac{1}{2}} \end{aligned} \tag{6}$$

Use of the substitutuion (y/b) = sin θ permits ready integration of (6)

The interelectrode potential and field distribution represented by (3) and (4) respectively are sketched in Fig. 3 for the case in which the gap and electrode width are equal. The relatively broad region of nearly uniform potential gradient is consistent with intuition. Note that the electric field is only about a third of V_o/gap width.

b. First Harmonic of the Field

In examining the diffraction effects of the interdigital structure, we limit our interest to the first harmonic of the applied field. This component extends deepest into the waveguide and provides the principal electro-optic interaction. In this paragraph we describe the relationship between the first harmonic term and the geometrical and electrical properties of the structures.

The electric field illustrated in Fig. 3 may be represented by a Fourier series with period 4a. The odd behavior about x = 0 assures that a sine series may be employed and the even behavior about x = ±a indicates that only odd terms in the series are nonzero. Thus (4) may be expressed

$$E_y = \sum_0^\infty A_n \sin(n + 1/2)\, \pi y/a \qquad (7)$$

where

$$A_n = (2/a)(V_o/2\cos^{-1}a/b)\int_b^a (y^2-b^2)^{-1/2}\sin(n+1/2)\pi y/a \; dy \qquad (8)$$

To obtain an approximate closed form for (8) when n = 0, the sine function will be modeled by the constant plus ramp function

$$\sin \pi y/2a \sim \sin \pi b/2a + (1-\sin \pi b/2a)(y-b)/(a-b) \qquad (9)$$

This model yields the correct value for the sine function at the singularity of the integrand, provides the same peak value of 1 at y = a, and generally underestimates the integral. Using the relations

$$\int (x^2-b^2)^{-\frac{1}{2}}\, dx = \ell n(x+(x^2-b^2)^{\frac{1}{2}})/b$$

$$\int x(x^2-b^2)^{-\frac{1}{2}}\, dx = (x^2-b^2)^{\frac{1}{2}}$$

integration of (8) yields

$$A_o/V_o/2a \sim 2[\sin \pi p/2 - p + (1-p^2)^{\frac{1}{2}}(1-\sin \pi p/2)/\cosh^{-1}p^{-1}]/(1-p) \qquad (10)$$

where p = ab/2a = finger width / distance between electrode centers. Equation (10) expresses the first harmonic of the electric field at the electrode plane normalized to the applied voltage/2a. The parameter $A_o/V_o/2a$ as expressed in (10) is shown sketched in Fig. 4. The underestimate provided by (10) may be expected to be significant only at small values of p.

The Fourier components of the electric field beyond the electrode plane exhibit an exponential behavior as may be deduced from Laplace's equation using the Fourier component of Φ. When the modulation frequency permittivities of all the layers are the same the solution for the electric field takes the form

$$\underline{E} = \sum_{0}^{\infty} A_n (\exp - (n+1/2)|z|/a)[\sin(n+1/2)\pi y/a \pm \cos(n+1/2)\pi y/a \ \hat{z}] \qquad (11)$$

Note that each component of $\underline{E}$ satisfies the equation $\nabla \cdot \underline{E}=0$ when the appropriate $\pm$ sign is taken in (11). By approximating the aperture field we have isolated the regions above and below the electrodes. The A_n both above and below the electrodes is expressed in (8).

In the presence of layers with differing permittivity the general expression for the electric field includes both increasing and decreasing exponentials in the form

$$E = \sum (C_n \exp -(n+1/2)z/a + D_n \exp(n+1/2)z/a)\sin(n+1/2)\pi y/a \ \hat{y}$$
$$+ (-C_n \exp -(n+1/2)z/a + D_n \exp(n+1/2)z/a)\cos(n+1/2)\pi y/a \ \hat{z} \qquad (12)$$

The coefficients in each region may be determined by matching the boundary conditions which are expressed

$$E_{y_n}\Big|_{z=0} = A_n \cdot E_{y_n} \text{ and } \varepsilon E_{z_n} \text{ continuous} \qquad (13)$$

Our interest lies in determining the solution for the first harmonic term inside the waveguide. Under proper design conditions the amplitude of the first harmonic will be small at the waveguide face opposite the electrodes. A simplified approximate solution to the linear boundary matching equations may therefore be obtained by applying (13) to the electrode interface and to the waveguide interface nearest the electrodes. This procedure results in the following expression for the first harmonic of the electric field in the waveguide

$$\underline{E}_o \sim A'_o(\exp -\pi z/2a)(\sin \pi y/2a \ \hat{y} - \cos \pi y/2a \ \hat{z}) \qquad (14)$$

with

$$A'_o/A_o = 2/[1+\varepsilon_2/\varepsilon_1)\exp \pi t/2a + (1-\varepsilon_2/\varepsilon_1)\exp -\pi t/2a] \qquad (15)$$

In (15), ε_1 is the permittivity of the isolation layer, ε_2 is the permittivity of the waveguide and t is the thickness of the isolation layer.

The parameter A'_o/A_o represents the loss in electric field intensity due to the presence of the isolation layer. When the waveguide itself has a high permittivity, as occurs with materials that exhibit the strongest electro-optic effects, there is a diminution of electric field intensity due to both the exponential decay and to the dielectric mismatch. Figure 5 shows a sketch of A'_o/A_o as expressed in (15) for two cases. In one the permittivity of the waveguide and isolation layer is the same, in which case the field decay is independent of the permittivity. The other curve shows the field decay for a nitrobenzene waveguide (ε_1 = 35.7) and a quartz (ε = 3.78) isolation layer. This decay is a moderately rapid function of the ratio of the layer thickness to the finger separation because of the large dielectric mismatch.

The parameters $A_o/V_o/2a$ and A'_o/A_o represent the amplitude of the first harmonic of the electric field at , respectively, the electrode plane and the waveguide interface nearest the electrodes. These parameters are functions of the geometric and electrical properties of the structure and enter into the evaluation and design of the diffraction modulator as will be further discussed in paragraph d.

c. Equivalent Circuit of the Diffraction Modulator

From the input electrical point of view, the diffraction modulator is principally a charge storage device and represents a capacitive load to an electrical system. A typical device length necessary to achieve full energy conversion of the optical signal might be a few millimeters. Within a factor related to optical and modulation frequency refractive indices, this length also represents the wavelength of the modulating signal at the frequency that corresponds to the optical transit time of the device. At modulation frequency wavelengths longer than a few millimeters, therefore, the diffraction modulator can be treated as a lumped element. A typical transit time is on the order of 10^{-11} sec. and the frequency below which the device may be considered to be lumped may be estimated as 10^{10} Hz.

The capacitance of the interdigital structure can be determined as the ratio of the total positive charge on the electrodes to the applied voltage. The total positive charge is equal to the product of the number of finger pairs by the charge on each finger. Equation (3) expresses the charge per unit length on one finger when the permittivity of all the regions is the same. Under the assumption that the regions above and below the electrodes are isolated, the charge on each electrode is one half the sum on either side and the capacitance may be expressed

$$C = \pi/2(1+\varepsilon_a/\varepsilon_b)(\cosh^{-1} a/b)^{-1} N \ell \varepsilon_b \qquad (16)$$

where N is the number of finger pairs, ℓ is the length, and ε_a and ε_b

refer to permittivities above and below the electrodes. Sample numerical values obtained for (16) when a = 2b are (0.08pf/mm)Nℓ with quartz on both sides and (0.42pf/mm)Nℓ with quartz on one side and nitrobenzene on the other.

The effect of an isolation layer between the electrodes and a high permittivity waveguide is to reduce the capacitance of the structure. To evaluate this effect the charge on an electrode may be recalculated from the electric field obtained upon solution of the boundary matching equations (13). As an approximation to this tedious procedure we may assume that the isolation layer is sufficiently thick so as to include the decay distance of all but the first harmonic of the electric field. As justification, recall that the next harmonic term decays at a rate three times as fast as the first. Referring to equation (12), the increase in charge on an electrode containing positive charge due to the presence of the waveguide may be expressed

$$\Delta Q = \varepsilon_1 \int_{-b}^{b} \Delta E_z \, dy \sim \varepsilon_1 (C_1 - D_1 - A_o) \int_{-b}^{b} \cos \pi y/2a \, dy$$

$$= \varepsilon_1 (C_1 - D_1 - A_o)(4a/\pi) \sin \pi b/2a \qquad (17)$$

where ε_1 is the permittivity of the isolation layer, A_o is the amplitude of the first harmonic of the electric field when the isolation layer is infinitely thick (eq./0), and C_1 and D_1 are the coefficients of the exponentially decreasing and increasing electric field components, respectively, in the presence of the waveguide.

To evaluate (17) the approximate boundary matching equations obtained from (13) by neglecting the effect of the waveguide boundary

more distant from the electrodes may be employed as in the previous paragraph. The coefficients C_1 and D_1 are solutions of the equations

$$C_1 + D_1 = A_o$$

$$C_1 \exp -\pi t/2a + D_1 \exp \pi t/2a = A'_o \qquad (18)$$

The resulting expression for (17) is found to be

$$\Delta Q = A_o(8a/\pi)(\sin \pi b/2a)(\varepsilon_2-\varepsilon_1)(\exp \pi t/2a)/[1+\varepsilon_2/\varepsilon_1)\exp \tau+(1-\varepsilon_2/\varepsilon_1)\exp -\tau] \qquad (19)$$

where $\tau = \pi t/2a$.

When the permittivity of the isolation layer is the same as that of the medium on the other side of the electrodes, the capacitance may be found as the sum of (16) and $\Delta Q/V_o$, i.e.,

$$C' = [\pi/\cosh^{-1}a/b + (2/\pi)(\varepsilon_2/\varepsilon_1-1)(\sin \pi b/2a)(A'_o/A_o)(A_o/V_o/2a)\exp -\tau] \; N \ell \varepsilon_1 \qquad (20)$$

The parameters A'_o/A_o and $A'_o/V_o/2a$ are shown in Figs. 4 and 5. The variation of the capacitance as expressed in (20) with the thickness of a quartz isolation layer and with finger separation is illustrated in Fig. 6. Results for guides of nitrobenzene and glass are shown. Equation (20) is not valid when the isolation layer thickness is small in comparison with $2a/\pi$ since the effect of the waveguide on the higher harmonics has been neglected. The curves in Fig. 6 are nevertheless continued into this region of isolation layer thickness. When the isolation layer is thin, equation (16) may be employed for the capacitance.

The equivalent circuit of the interdigital structure is very nearly a simple capacitor shunting the input terminals to the interdigital structure. The capacitance is expressed in (20). When the loss tangent of the waveguide material is not negligible, however, the equivalent circuit is more complex. It must account for the fact that all electric field lines that pass through the waveguide first pass through the isolation layer. The observable consequence of this phenomenon is a low frequency cutoff for the modulator.[2] To generate an accurate equivalent circuit requires an extensive field analysis, and because of the geometrical arrangement the resulting circuit may be expected to be quite complex and to contain elements that are frequency dependent. In the interest of developing a simple equivalent circuit that illustrates the basic features of the frequency behavior we present the circuit shown in Fig. 7.

The equivalent circuit of Fig. 7 is based on physical arguments that may be described in terms of the electrode configuration that is also illustrated in Fig. 7. If we identify equipotential surfaces such as the dotted ellipses of Fig. 7, the regions inside ellipse 1, outside ellipses 1 and 2, and inside ellipse 2 are in series and result in series elements in the equivalent circuit. We assume that the ellipse with minor axis of half length t is an approximate equipotential surface. From equation (3) we deduce that the major axis is of half length $2\sqrt{b^2 + t^2}$ and from (2) and (3) that the potential of this surface is

$$\Phi_1 \sim \frac{V_o}{2} \frac{\cosh^{-1}\sqrt{b^2+t^2}/b}{\cosh^{-1} a/b} = \frac{V_o}{2} \frac{\sinh^{-1} t/b}{\cosh^{-1} a/b} \qquad (21)$$

From equation (5) we deduce that the capacitance per unit length that is denoted C_a is

$$C_a = \frac{1}{4}\frac{\Phi_1}{Q} = \frac{1}{4}\frac{(2\pi\varepsilon_1)}{\sinh^{-1} t/b} \tag{22}$$

In series with the capacitance C_a is a set of parallel elements. C_b may be determined by noting that the series combination C_a-C_b-C_a provides 1/4 the capacitance expressed in (16) with $\varepsilon_a = \varepsilon_b = \varepsilon_1$. Thus

$$\frac{1}{C_a} + \frac{1}{C_b} + \frac{1}{C_a} = \left[\frac{1}{4}\ \frac{\pi}{\cosh^{-1} a/b}\ \varepsilon_1\right]^{-1} \tag{23}$$

The other parallel elements C_c and C_d are intended to represent contributions from the portion of the field which passes through the isolation layer and the waveguide, respectively. Since the field lines do not pass parallel to the interface at t, the subdivision into C_c and C_d is clearly only an approximation. The parallel combination of C_c and C_d may be computed by identifying the series combination C_a-(C_c||C_d)-C_a with half of C' expressed in (20) less the contribution to (20) from the region below the electrodes. Thus

$$\frac{1}{C_a} + \frac{1}{C_c+C_d} + \frac{1}{C_a} = \left[\frac{1}{2}\left(C' - \frac{\pi/2}{\cosh^{-1} a/b}\ \varepsilon_1\right)\right]^{-1} \tag{24}$$

The final equation required for determination of the capacitances of the equivalent circuit may be obtained in approximate fashion by equating C_d with the energy stored in the waveguide region of the structure normalized to half the square of the potential difference

between the dotted electrodes. In accordance with our assumption that only the lowest order harmonic of the electric field significantly penetrates the waveguide we may express C_d as

$$C_d \simeq \frac{1}{2}\varepsilon_2 \int (E_y^2 + E_z^2)\, dV \Big/ \frac{1}{2}(V_o - 2\Phi_1)^2$$

$$\simeq 2\varepsilon_2 \int_0^{2a}\int_0^{\infty} A'^2_o \sin^2 \pi y/2a\, e^{-\pi z/a} \Big/ (V_o - 2\Phi_1)^2$$

$$\simeq \frac{\varepsilon_2}{2\pi}\left(\frac{A'_o}{A_o}\right)^2\left(\frac{A_o}{V_o/2a}\right)^2\left(1 - \sinh^{-1} t/b \cosh^{-1} t/b\right)^{-2} \tag{25}$$

Equations (22) - (24) define the capacitances of the equivalent circuit of Fig. 7. The bold assumptions made in generating the circuit render the circuit only a rough approximation. To complete the equivalent circuit, the conductance G_d, which represents the absorption due to the finite conductivity of the waveguide, material may be expressed in terms of the capacitance C_d as

$$G_d = \frac{\sigma}{\varepsilon_2} C_d = w \frac{\varepsilon_2''}{\varepsilon_2'} C_d = w \tan\delta\, C_d \tag{26}$$

where σ and $\tan\delta$ are the conductivity and loss tangent of the waveguide material, respectively. The behavior of the loss tangent for nitrobenzene will be discussed in Chapter 3. At low frequencies the value of σ for pure nitrobenzene is $O(3\times10^{-10}$ V/cm).

d. Frequency Behavior of the Diffraction Modulator

The spectral behavior of the diffraction modulator is characterized

by a low frequency cutoff due to the assumed finite resistivity of the waveguide region as well as high frequency cutoffs due to either relaxation effects in the waveguide material or circuit effects that arise as a result of the presence of matching elements. Relaxation effects are discussed in Chap. 2. Our concern in this section lies with evaluation of the cutoff frequencies and device figure of merit.

The low frequency cutoff of the modulator corresponds to a situation in which the modulating electric field in the waveguide region is reduced to low values because of the presence of induced charges at the interface between the waveguide and the isolation layer. At dc the modulating field is zero in the guide. The approximate equivalent circuit shown in Fig. 7 provides an estimate of the frequency at which substantial electric field appears in the waveguide. The field in the waveguide is proportional to the voltage across the conductance G_d and this voltage reaches 0.707, its midband range, when the impedance relation

$$\left| \frac{[jw(C_c+C_d) + G_d]^{-1}}{(jwC_a/2)^{-1} + [jw(C_c+C_d) + G_d]^{-1}} \right| = 0.707 \qquad (27)$$

is achieved. For thin isolation layers the capacitance C_a is large in comparison with C_c+C_d. The low frequency cutoff expressed in (27) is therefore approximately

$$f_{L.F.C.} = \frac{G_d}{\pi C_a} = \frac{\sigma}{\varepsilon_2} \frac{C_d}{\pi C_a} \qquad (28)$$

The frequency indicated by (28) can lie in the range from a few Hz to

values in the KHz range depending on σ/ε_2 for the waveguide material.

Beyond the low frequency cutoff the modulator may be modeled as a capacitor of capacitance C', at least to frequencies at which G_d becomes appreciable due to relaxation effects. To achieve a certain depth of optical modulation we require a prescribed voltage, denoted V_p, between the fingers of the interdigital structure, i.e., across the capacitance C'. The bandwidth of the modulator is dependent on the voltage transfer function of the amplifier including associated matching elements that is used to excite the modulator. It is customary[5,6] in evaluating the performance of optical modulators to consider simple circuits of the kind illustrated in Fig. 8, in which the amplifier is characterized by an output resistance R_s. For experimental purposes R_s is frequently taken to be 50Ω for purposes of matching to available coaxial cables.

Defining the cutoff frequency of the lumped circuits of Fig. 8 as the frequency at which the voltage transfer function reduces to $1/\sqrt{2}$ its peak value, the baseband modulator is readily found to have a cutoff frequency

$$f_{HFC} = 1/2\pi R_s C' \tag{29}$$

while the tuned modulator has a bandwidth

$$BW/f_o = (BW)\frac{\sqrt{LC'}}{2\pi} = 2\pi f_o R_s C' \tag{30}$$

These equations indicate that to achieve bandwidths of about 3 GH_z when $R_s = 50\Omega$, baseband modulator capacitance must be approximately one

picofarad and the tuned modulator capacitance at a center frequency of 3 GH_z must also be one picofarad. On the basis of the capacitance values indicated in Fig. 6, wide bandwidths can only be achieved if the number of finger pairs is kept small and if the lengths of the fingers do not exceed a few millimeters.

More elaborate matching networks can be used to extend the bandwidth of the voltage transfer functions. These matching networks can include sections of transmission line as indicated in Fig. 8 and as discussed, for example, by Reeder and Sperry.[7] For device comparison, however, it is customary to employ the lumped models of Fig. 8 and to describe a Figure of Merit as the ratio of the power delivered to the resistor R_s at the cutoff (or midband) frequency to the cutoff frequency (or the bandwidth). When the voltage across the capacitor C' is V_p the power delivered to R_s for the parallel or series circuits of Fig. 8 is, at any frequency ω, respectively

$$P_R = \frac{1}{2} V_p^2/R_s \quad \text{or} \quad P_R = \frac{1}{2} \omega^2 C'^2 R_s V_p^2 \tag{31}$$

The value of R_s is expressed in terms of the bandwidth in (29) and (30). Evaluating ω at ω_c or ω_o, the resulting Figure of Merit is found to be

$$\frac{P_R}{f_c} \left(\text{or } \frac{P_R}{BW}\right) = \pi C' V_p^2 \tag{32}$$

The expression (32) indicates that a device that has only a few picofarads of capacitance and requires only a few volts to extinguish the optical signal can provide a bandwidth of 10^{10} Hz at modulation powers below a watt.

Evaluation of the Figure of Merit requires specification of V_p, the voltage we take to be that required to fully extinguish the undiffracted beam in a diffraction modulator. In linear waveguides V_p would be the voltage required to convert from the wave from one mode to another or from one polarization to another. In a thin film diffraction modulator there is generally present both spatial diffraction and TE-TM mode conversion. A full analysis of conversion effects in these structures has not been published as yet, but is under investigation in our laboratory. To estimate the value of V_p we may follow the procedure of Polky and Harris[2] which consists of neglecting the polarization rotation and assuming that the spatial index variation is a sinusoid whose peak value is half the difference between the peak index change induced by E_z and by E_y in the waveguide. For Kerr liquids this procedure yields a sinusoidal index variation of the form

$$\Delta n = \frac{1}{2} K\lambda A_o'^2 \, e^{-\pi z/a} \sin \pi y/a \tag{33}$$

where K is the Kerr constant of the liquid and A_o' is the peak amplitude of the modulating field in the waveguide.

The wave index variation provided by (33) may be estimated as the average of (33) through the waveguide and if we assume that the decay distance is comparable to the film thickness t_f we find

$$\Delta n_w \sim \frac{1}{2} \frac{a}{\pi t_f} K\lambda A_o'^2 \sin \pi y/a \equiv \alpha \sin \pi y/a \tag{34}$$

Note that the averaging factor $(a/\pi t_f)$ must never be taken greater than

unity. When the wave is incident on the modulator at the Bragg angle the relative intensity of the undiffracted wave is expressed

$$I = \cos^2(k_o \alpha L) \tag{35}$$

where L is the length of the modulator. Complete extinction of the undiffracted beam therefore occurs when $k_o \alpha L = \pi/2$ or when

$$A_o'^2 = \frac{\pi t_f}{aK\lambda} \frac{\pi}{k_o L} \tag{36}$$

Multiplying (36) by the unit factors $(V_p/2a)^2/(V_p/2a)^2$ and $(A_o'/A_o)^2$ we obtain an expression for V_p in terms of previously defined parameters, viz.,

$$V_p^2 = \frac{(2a)^2}{(2a/\pi t_f)(A_o'/A_o)^2 (A_o/V_p/2a)^2 KL} \tag{37}$$

The Figure of Merit obtained by placing (37) in (32) and identifying the number of finger pairs as $N = W/4a$ where W is the width of the device is

$$\frac{P_R}{BW} = \frac{P_R}{f_c} = \pi \left(\frac{C'}{nL} \right) \cdot \frac{Wa}{(2a/\pi t_f)(A_o'/A_o)^2 (A_o/V/2a)^2 K} \tag{38}$$

The parameters (C'/nL), (A_o'/A_o), and $(A_o/V/2a)$ are depicted in Figs. 4, 5, and 6 as functions of the device parameters. To obtain an estimate of the Figure of Merit when the Kerr liquid is nitrobenzene ($K = 3.6\times10^{-12}$) we may assume that the various factors in the denominator of (38) are unity, with the exception of K, and take $(C'/nL) \sim 0.2$ pf/mm = 200 pf/m. The resulting Figure of Merit is

$$\frac{P_R}{BW} \sim 0[100\ W(2a)] \tag{39}$$

Note that when the finger separation is on the order of a micron ($2a \sim 10^{-6}$), the Figure of Merit is on the order of (10^5W) watts/GH_z and device widths of a few microns are required if it is desired to modulate over a GH_z bandwidth using powers of less than a watt.

For a non-polar liquid like CS_2 the Kerr constant is approximately 1/100 that of nitrobenzene. Taking into account the lower associated permittivity, the Figure of Merit for a CS_2 device would be greater than that of a nitrobenzene device by a factor of 10. It should be noted that the Figure of Merit for Kerr liquids is independent of device length. The maximum voltage that can be applied to the device is limited, however, by breakdown considerations. The extent to which the large fringing electric field at the edges of the electrodes limit the voltage is uncertain at present and must be considered an outstanding design question. Equation (37) relates the device length to the applied voltage and may be used to establish the necessary device length once the maximum allowable voltage is established. Since the Figure of Merit is independent of the device length, appropriate design would fix the length of the device to the maximum allowed by transit time considerations in order to minimize V_p.

II. Dielectric Properties and Kerr Constants of Fluids

The dielectric properties of fluids at microwave frequencies have been studied extensively and appear to be well understood. An extensive body of literature is available on the subject,[8-13] and nitrobenzene is well represented in the experimental data. The literature is primarily concerned with the properties of dielectrics and the molecular structure of liquids.

For polar liquids the permittivity, polarization, dielectric constant, etc. are nearly all the result of dipole rotation and alignment. In a great number of cases the dipole moment of the molecule is much larger than any induced moment, and the dipole may be considered rigid. With increasing frequency the dynamics of the dipole reorientation eventually play a role.

By its size, shape, and dipole strength, the molecule interacts with its neighbors; and the structure of the fluid determines the dynamics with which the dipole reorientation occurs. Debye (e.g., see Hill[8]) found that in most materials the dispersion could be characterized by a simple relaxation process with a single time constant. Such a time constant ranges from the high audio for some vulcanized rubber to the 10 p sec range for many simple polar organic liquids. Relevant equations that characterize the Debye model are presented in Table 1 and sample complex dielectric constants are presented in Fig. 9. Many materials do depart from this model; some have an apparent spread in the time constant, τ, and others may have two or more distinct time constants.

For our purposes this model adequately describes the behaviour

of most polar fluids likely to be used. Non-polar fluids, on the other hand, do not show this relaxation behavior, but will certainly show resonance absorption and dispersion at molecular spectral frequencies. These frequencies are generally much higher than those of polar relaxation in fluids (and higher than frequencies of interest for light modulation).

Several researchers have reported measurements on nitrobenzene.[14-17] Their data is in general agreement although some differences appear. Fig. 9 shows the basic features of the complex dielectric constant for nitrobenzene. The curves are only slightly stylized. They are drawn assuming a pure Debye model, the parameter values are rounded off, and they represent the curves in the temperature range 20-25° C. For higher temperatures the time constant becomes shorter and the loss peak moves to somewhat higher frequency. Clark[14] reported a characteristic frequency of 5.7 GHz for 55 deg. C.

From Fig. 9 we may derive views of how nitrobenzene will behave at frequencies of interest in connection with optical modulation. The permittivity decreases dramatically in the 1 to 10 GHz range and the loss tangent approaches and exceeds unity. In accordance with equation (26), the conductance of the modulator rises to values on the order of ωC_d and there is rapid associated heating of the device.

Data is also available for other polar fluids.[14-19] The general situation is that most polar liquids have time constants not too different from that of nitrobenzene. As for the electro-optic properties of polar liquids in the microwave range, the change in permittivity with frequency

may be expected to represent an associated reduction in Kerr constant. This is because the Kerr constant reflects the anisotropic optical polarizability of the molecule, which for polar moelcules is invariably greatest along the axis of the dipole. The Kerr effect and the dielectric constant have a common source -- the reorientation of the molecular dipole. Thus we may expect that all materials which have a large Kerr constant because of their polar nature will have that constant decrease rapidly with frequency in the dispersion region. Kerr constants available in the literature [20-24] are intended to be for static fields (even though a pulsed HV may have been used). There do not appear to be reports of effective Kerr constants at high frequencies.

It appears likely that polar fluids will not be useful for diffraction modulators at microwave frequencies, even though these include those of highest Kerr constant. Only a casual survey has been made of about six material with the highest Kerr constants--all have a large dipole moment.[19] A more systematic search may be justified to support this conclusion.

Liquids of useable Kerr constant at microwave frequencies do exist. Carbon disulfide is the tried and proven one.[25-28] It has zero dipole moment and is essentially lossless to beyond 10 GHz. It is likely that other useful liquids could be found.

III. Excitation of Modulators

The effective use of optical integrated circuits arises when a communication system involves several channels requiring gigahertz or near gigahertz bandwidths. At lower overall bandwidth requirements, LED-multimode fiber bundle and space duplexed versions of these systems can suffice. When the required bandwidth is sufficient to justify use of integrated optics, the associated electronic modulation scheme will involve employment of microstrip lines to carry electronic signals to modulators or from detectors.

Of the various microstrip designs [29], the slot transmission line is probably the one most directly applicable to integrated optical systems. Fig. 10 is an illustration of how the slot line might be used in a two channel integrated optical system. Associated with the slot line will be matching resistive or combined inductive-resistive components. The matching components can be deposited on the isolation layer as is the slot line. Further integration of the electronic components is, of course, desirable, but is a problem whose solution must await future developments in the design of integrated optical components. The compatibility of the integrated optical and electronic substrates is, of course, of concern in that regard. In the present experimental stage of integrated optical modulator development, the use of slot microstrip coupled to coaxial inputs appears to be a useful technique for applying high frequency electronic signals to devices.

Conclusion

The design of wide bandwidth electro-optic modulators requires minimization of the dimensions of the active waveguide and associated electrodes and isolation layers. As each of these dimensions approaches the wavelength of light, careful design is required to avoid diminution of device effectiveness. The potential for using low-cost liquid guides as hybrid modulator components is limited by polar relaxation effects to the sub-gigahertz frequency range. Development of solid-state thin film modulator components is clearly warranted.

REFERENCES

1. D. F. Nelson and F. K. Reinhart, Appl. Phys. Lett. 5, 148 (1964); F. K. Reinhart, J. Appl. Phys. 39, 3426 (1968); D. Hall, A. Yariv, and E. Garmire, Opt. Comm. 1, 403 (1970) and Appl. Phys. Lett. 17, 127 (1970).

2. D. P. GiaRusso and J. H. Harris, Electrooptic modulation in a thin film waveguide, Appl. Optics 10, 2786L (1971).

3. J. N. Polky and J. H. Harris, Interdigital electro-optic thin-film modulator, Appl. Phys. Lett. 21, 307 (1972).

4. R. Plonsey and R. E. Collin, Principles and Applications of Electromagnetic Fields, p. 153, McGraw-Hill, New York (1961).

5. I. P. Kaminow and E. H. Turner, Electrooptic light modulators, Proc. IEEE 54, 1374 (1966).

6. R. T. Denton, F. S. Chen, and A. A. Ballman, Lithium tantalate light modulators, J. Appl. Phys. 38, 1611 (1967).

7. T. M. Reeder and W. R. Sperry, Broad band coupling to high-a resonant loads, IEEE Trans. MTT 20, 453 (1972).

8. N. E. Hill, et al., Dielectric Properties and Molecular Behaviour, Van Nostrand-Reinhold, London (1969).

9. A. R. von Hipple, Dielectrics and Waves, John Wiley, New York (1954).

10. J. H. Calderwood, editor, Complex Permittivity, English University Press, London (1971).

11. R. H. Cole, "Theories of dielectric polarization and relaxation", in Progress in Dielectrics, Volume 3, pp. 47-99, Heywood Company, London (1961).

12. K. H. Illinger, "Dispersion and absorption of microwaves in gases and liquids", in Progress in Dielectrics, Volume 4, Heywood Company, London (1962).

13. C. W. N. Cumper, A. Melnikoff, and B. F. Rosciter, "Absorption of microwave radiation by solutions"; Pt. 1, "Determination of electric dipole moments and relaxation times", Trans. Faraday Soc., Volume 65, Pt. 11, pp. 2892-2899, November (1969).

14. G. L. Clark, Dielectric properties of nitrobenzene in the region of anomalous dispersion, J. of Chem. Physics, 25, n1, 125-129 (1956).

15. J. Ph. Poley, Microwave dispersion of some polar liquids, Applied Sci. Research (Netherlands), B4, n4, 337-387 (1955).

16. C. Demau, G. Delbos, and G. Vicq, Microwave study of the dielectric relaxation of mono-substituted derivatives of benzene as a function of temperature, and the determination of the corresponding molecular constants, Compt. Rendus Acad. Sci. (Paris), 272, n26, 1481-4 (1971). (In French).

17. C. Demau, G. Delbos, and G. Vicq, Study of dielectric relaxation of mono-substituted benzene derivatives in X and S bands in liquid phase as a function of temperature, J. de Chimie Physique, 69, n2, 212 (1972). (In French).

18. I. J. Makhiya and A. L. Dawar, Dielectric constants and tan-delta for some low loss liquids, Defence Science Journal (India), 21, n3, 187-92, July (1971).

19. F. Buckley and A. A. Maryott, Tables of Dielectric Dispersion and Data for Pure Liquids and Dilute Solutions, National Bureau of Stds. Circular 589, November (1958).

20. International Critical Tables of Numerical Data, Physics, Chemistry and Technology, NBC - NAS - McGraw Hill, New York, Volume 7; "Electric and Magnetic Binefringence, pp. 109-113 (1930).

21. Am. Inst. Physics Handbook, D. E. Gray, editor, 3rd edition, McGraw Hill, New York, Table GM-3, pp. 6-187 (1963).

22. C. G. Le Fevre and B. J. W. Le Fevre, The Kerr effect. Its measurement and applications in chemistry, Rev. of Pure and Appl. Chem., 5 n4, 261-318 (1955).

23. S. M. Lee and S. M. Hauser, Kerr constant evaluation of organic liquids and solution, Rev. of Sci. Instrum., 35, n12, 1679-1681, December (1964).

24. A. D. Pearson, W. R. Northover, and E. A. Chandros, Kerr effect in substituted aromatic nitro compounds, J. of Appl. Physics, 41, n6, 2576-2580, May (1970).

25. A. J. Chenowith, Carbon disulphide traveling-wave Kerr cells, Applied Optics, 5, 1652 (1966).

26. A. J. Chenowith and O. L. Gaddy, Microwave frequency light modulation with traveling-wave carbon disulphide Kerr cells, Proc. I.E.E.E., 54, n6, 877 (1966). (Letter).

27. O. L. Gaddy, D. F. Holshauser, and R. E. Stanfield, Microwave and electro-optical properties of carbon disulphide, Proc. of Third Quantum Electronics Conf. (Paris, 1963), P. Grivet and N. Bloemberger, eds., Columbia University Press, New York, pp. 1679-1686 (1964).

28. D. F. Holshauser, H. Von Foerester, and G. L. Clark, Microwave modulation of light using the Kerr effect, J. Opt. Soc. of Am., 51, n12, 1360-1365, December (1961).

29. M. V. Schneider, Microstrip lines for microwave integrated circuits, B.S.T.J., 48, 1421 (1969).

FIGURES

Figure 1. Cross section of diffraction modulator. Electrodes shown as dark strips are of width 2b and are a distance 2a between centers. The isolation layer is of thickness t and the waveguide is shown shaded.

Figure 2. (a) General shape of the equipotential surfaces near one electrode of the diffraction modulator. (b) Concentric elliptic model used to estimate the electric field between electrodes in the plane of the electrodes.

Figure 3. Approximate potential distribution Φ and electric field component E_y in the plane of the electrodes of a diffraction modulator.

Figure 4. Approximate amplitude of the first harmonic of the Fourier expansion of E_y and E_z in the plane of the electrodes, A_o, normalized to the ratio of the applied voltage V_o to the distance between adjacent electrode centers vs. relative finger width $p = 2b/2a$.

Figure 5. Approximate amplitude of the first harmonic of the Fourier expansion of E_y and E_z in the plane of the waveguide interface nearest the electrodes vs. normalized isolation layer thickness $\tau = 1.57t/a$. The permittivity of the isolation layer is ε_1 and that of the waveguide is ε_2.

Figure 6. Approximate capacitance of a diffraction modulator normalized to the number of finger pairs and the length and expressed in picofarads/mm vs. normalized isolation layer thickness $\tau = 1.57t/a$ and relative electrode width $p = 2b/2a$.

Figure 7. (a) Cross section of diffraction modulator with electric circuit components used to estimate low frequency cutoff properties shown superposed. The waveguide is the shaded area and the dotted ellipses are approximate equipotential surfaces that surround the electrodes and extend to the surface of the waveguide. (b) Approximate equivalent electric circuit per finger pair and per unit length of diffraction modulator as obtained from Fig. 7a. (c) Approximate midband and high frequency equivalent electric circuit of the diffraction modulator.

Figure 8. Examples of electric circuit configurations in which the diffraction modulator represented by capacitance C' can be connected to a voltage source with output inpedance R_s. (a) Baseband configuration. (b) Passband configuration. (c) Baseband configuration coupled through a transmission line of characteristic impedance R_s. (d) Passband configuration coupled through a transmission line.

Figure 9. (a) Debye and Cole-Cole circle representations of complex dielectric constant of a singly resonant polar liquid. (b) Debye representation for nitrobenzene. (c) Cole-Cole representation for nitrobenzene including data points.

Figure 10. Experimental modulator design showing two slot microstrip lines (shaded) with associated interdigital structure and terminated in matching resistive or inductive-resistive load. Linear optical waveguides are transverse to the lines. Dimension "a" is on the order of microns while "b" is on the order of millimeters.

TABLES

Table 1. Parameter definitions for Debye and Cole-Cole circle representations of the permittivity of a singly resonant polar liquid.

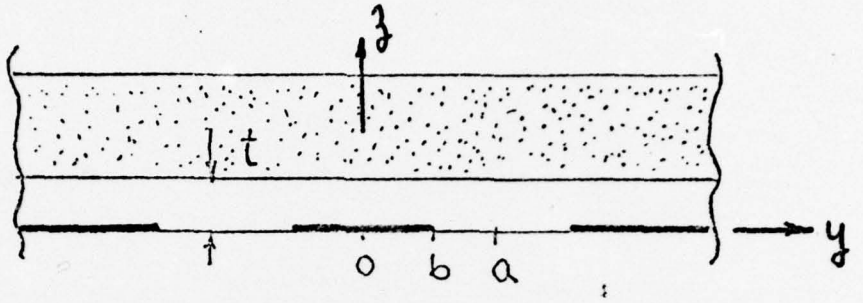

Figure 1

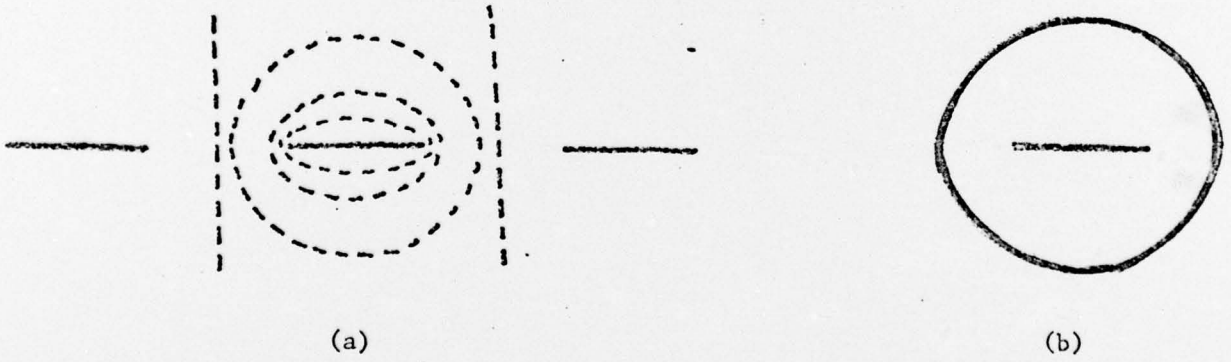

(a) (b)

Figure 2

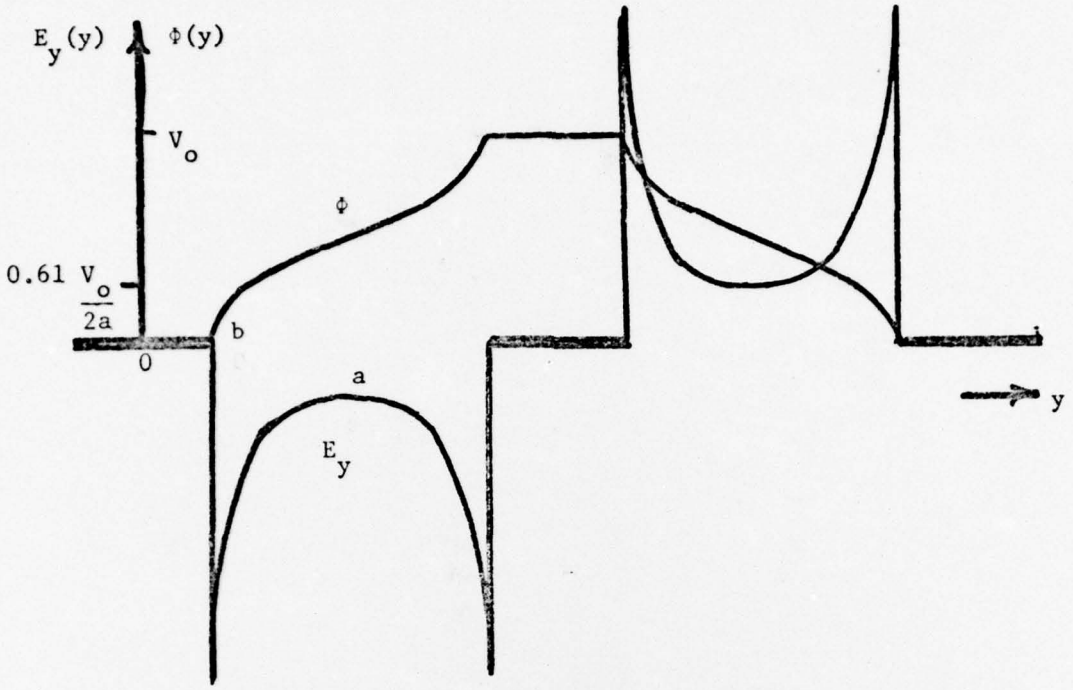

Figure 3

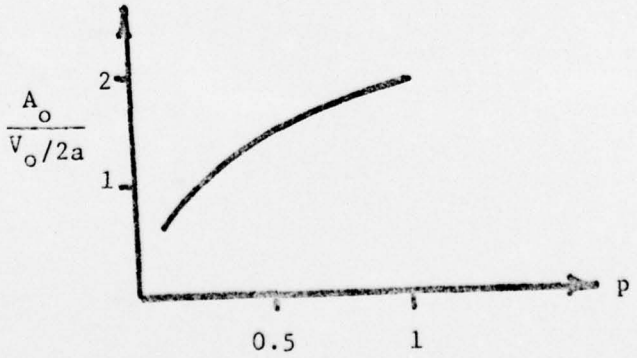

Figure 4

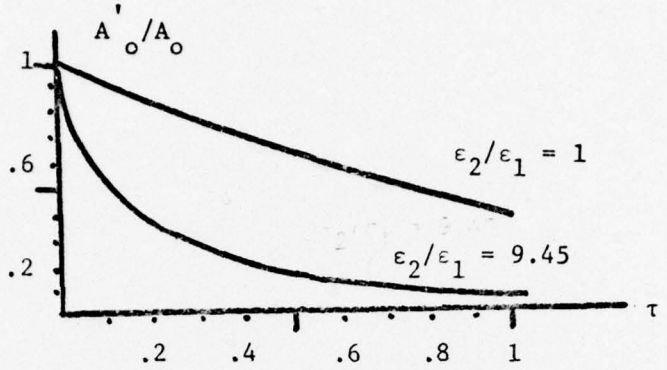

Figure 5

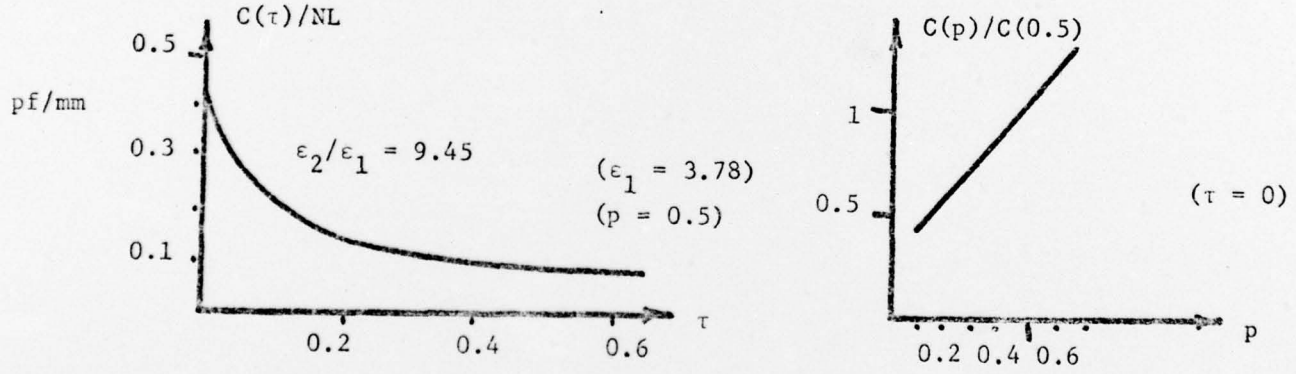

Figure 6

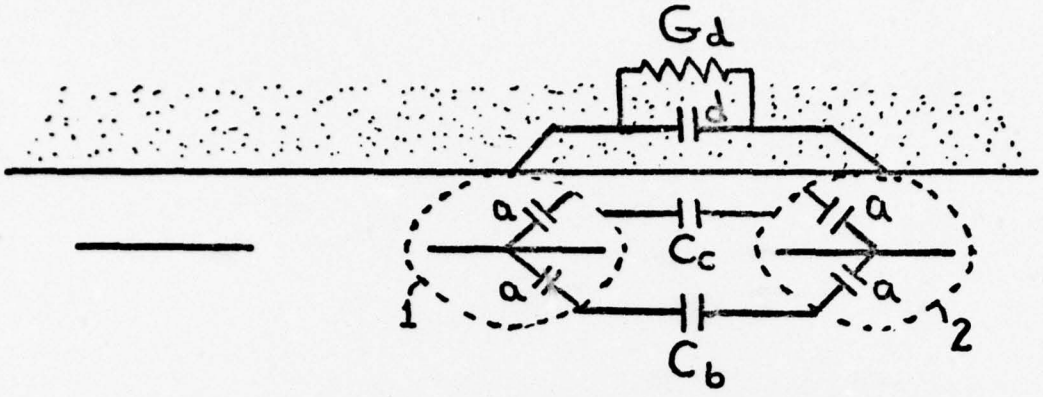

(a)

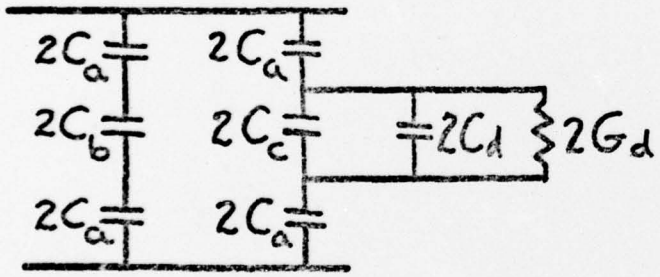

(b)

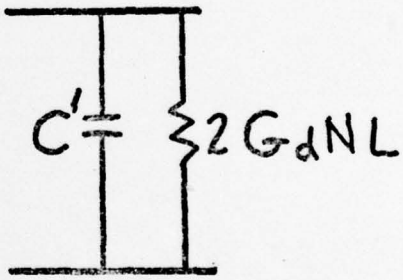

(c)

Figure 7

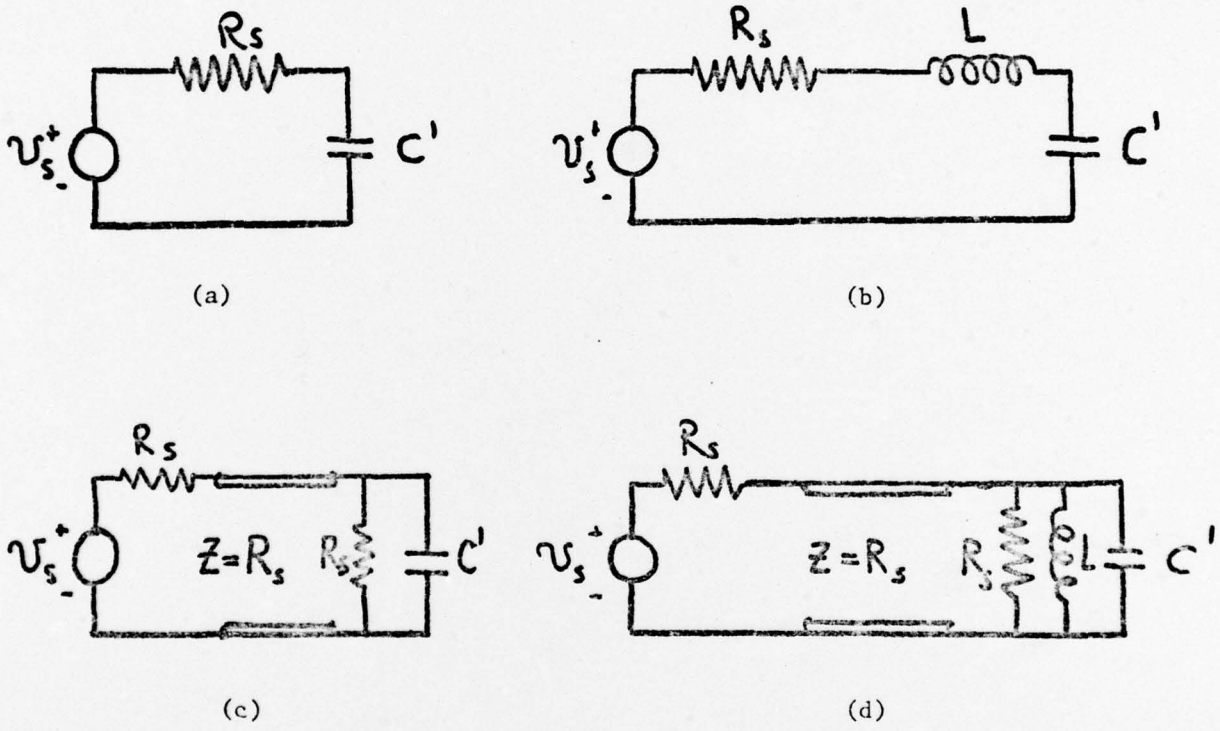

Figure 8

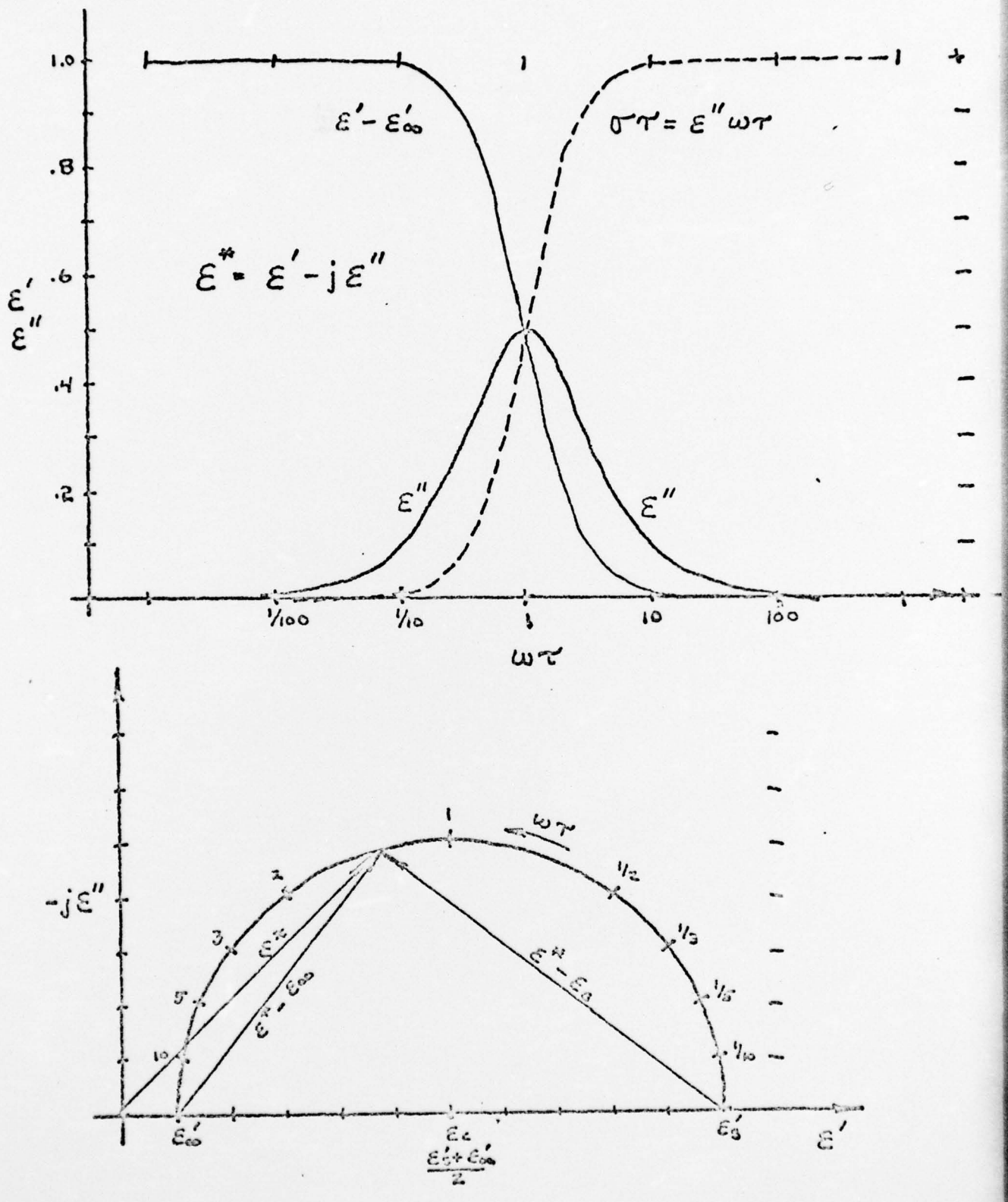
1.0
.8
.6
.4
.2
ε'
ε''
ε'-ε'∞
στ = ε''ωτ
ε* = ε'-jε''
ε''
ε''
1/100
1/10
1
10
100
ωτ
-jε''
ε'∞
ε'-ε'∞
ε''
ε''-ε∞
ε'
ωτ
1
2
3
5
10
1/2
1/3
1/5
1/10
ε'∞
εc
(ε'∞+ε∞)/2
ε∞
ε'

Figure 9.0

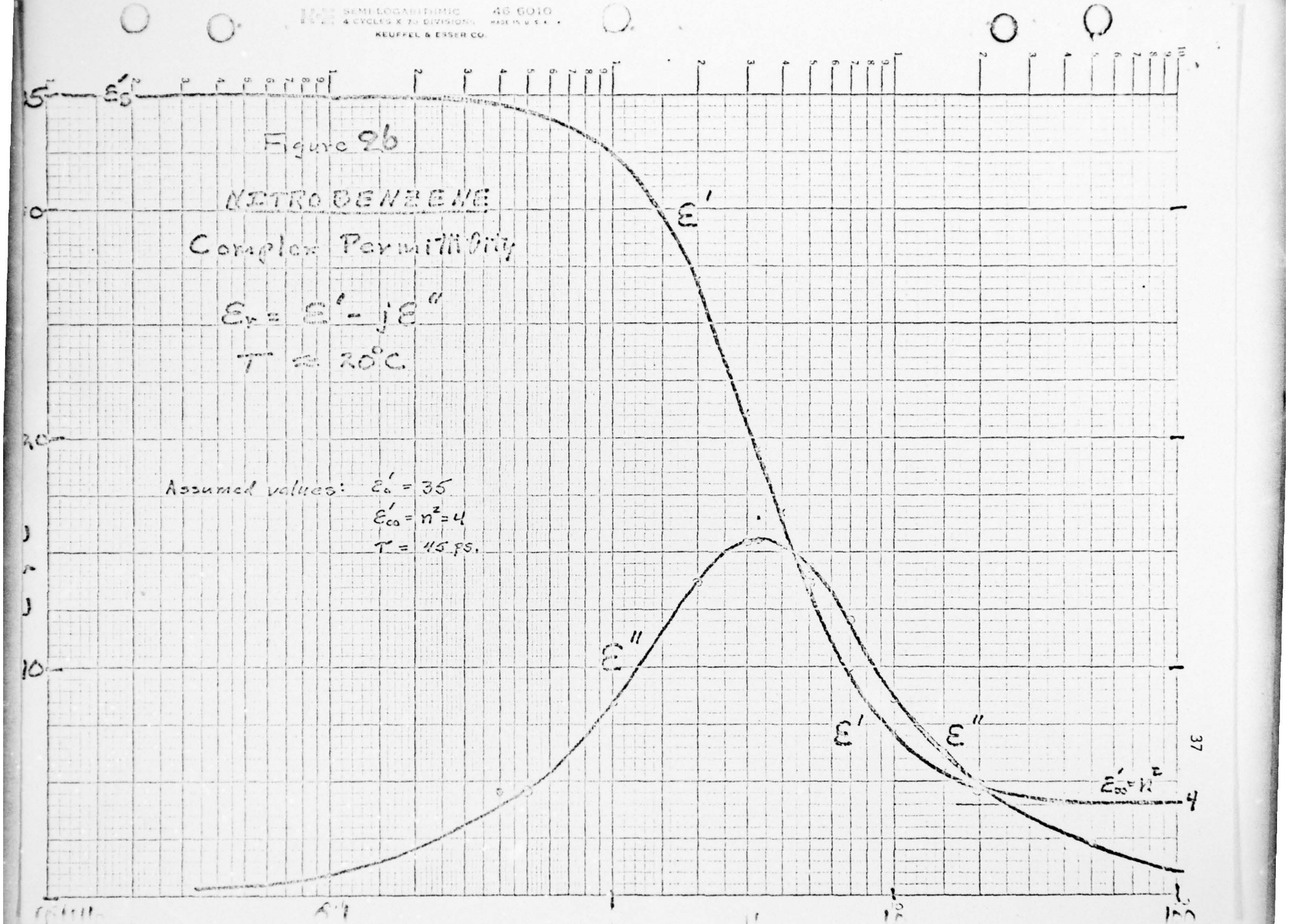
SEMI-LOGARITHMIC 46 6010
4 CYCLES X 70 DIVISIONS
KEUFFEL & ESSER CO.
Figure 9b
NITROBENZENE
Complex Permittivity
$\varepsilon_r = \varepsilon' - j\varepsilon''$
$T = 20°C.$
Assumed values: $\varepsilon_0' = 35$
$\varepsilon_{\infty}' = n^2 = 4$
$\tau = 115$ ps.
ε_0'
ε'
ε''
ε'
ε''
$\varepsilon_\infty' = n^2$
35
30
20
10
4
37

Figure 9c

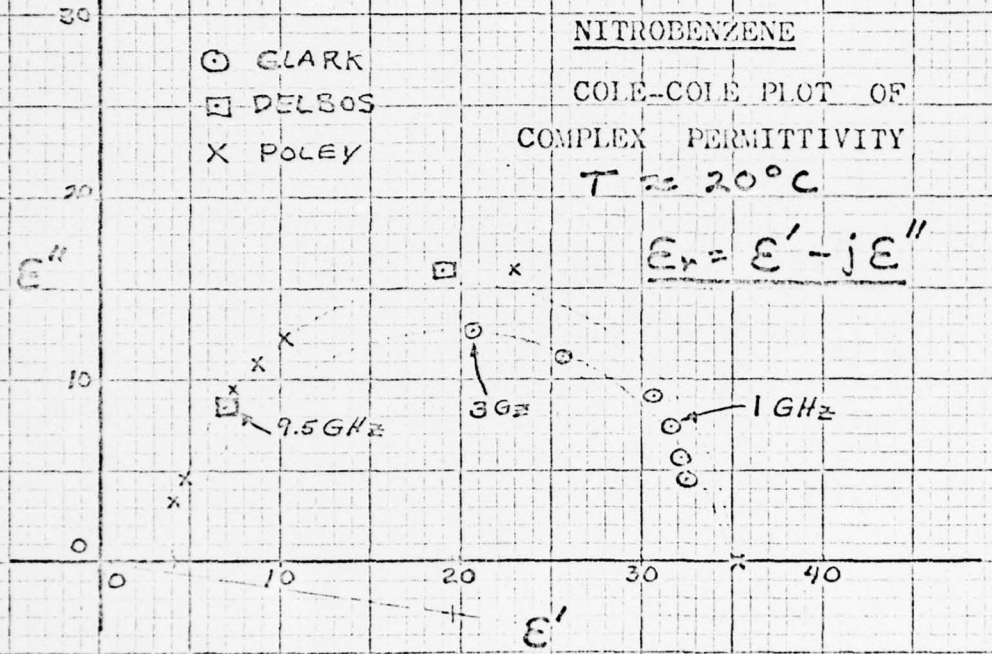

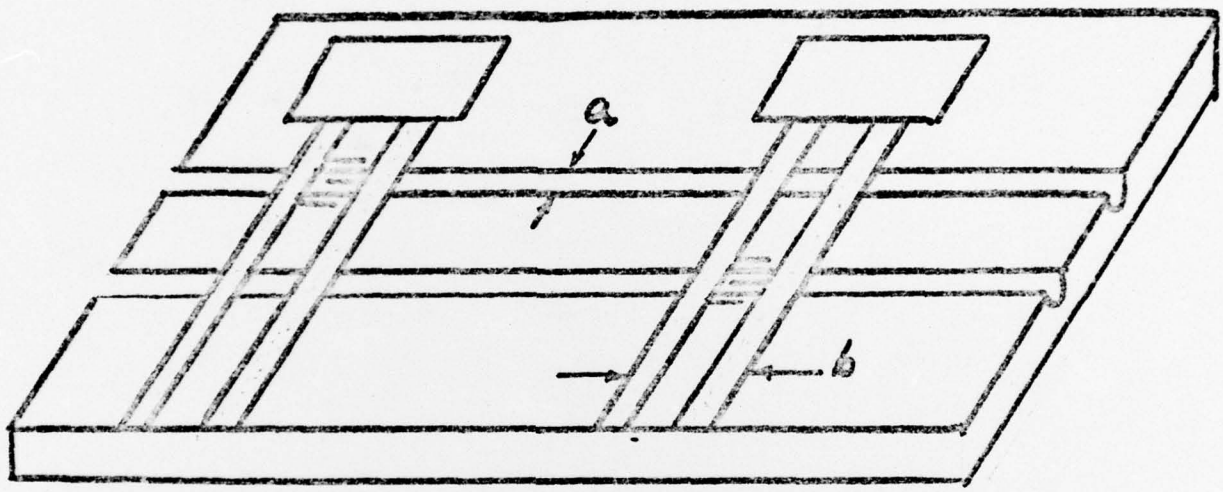

Figure 10

Table 1

COMPLEX RELATIVE PERMITTIVITY: $\varepsilon^* = \varepsilon' - j\varepsilon''$

DEBYE MODEL: $\varepsilon^*(\omega) = \varepsilon_\infty + \frac{\varepsilon_s - \varepsilon_\infty}{1 + j\omega\tau}$

REAL PART: $\varepsilon'(\omega) = \varepsilon_\infty + \frac{\varepsilon_s - \varepsilon_\infty}{1 + \omega^2\tau^2}$

IMAGINARY PART: $\varepsilon''(\omega) = \frac{\varepsilon_s - \varepsilon_\infty}{1 + \omega^2\tau^2} \cdot \omega\tau$

PARAMETERS: $\varepsilon_s \equiv \varepsilon'(\omega \to 0)$

$\varepsilon_\infty \equiv \varepsilon'(\omega \to \infty)$ $\qquad \omega \equiv 2\pi f$

$\tau =$

COLE & COLE CIRCLE RRESENTATION:

Definitions: $\varepsilon_c \triangleq \varepsilon'(\omega\tau = 1) = \frac{\varepsilon_s - \varepsilon_\infty}{2}$

$R \triangleq \frac{\varepsilon_s + \varepsilon_\infty}{2}$

THEN, $\varepsilon'(\omega) - \varepsilon_c = R\left(\frac{1 - \omega^2\tau^2}{1 + \omega^2\tau^2}\right)$

$\varepsilon''(\omega) = R\left(\frac{2\omega\tau}{1 + \omega^2\tau^2}\right)$

A CIRCLE IN THE $\varepsilon', \varepsilon''$ PLANE, WITH CENTER AT ε_c AND RADIUS R; $\omega\tau$ IS A PARAMETER ALONG CIRCUMFERENCE.